# OPTICAL PROPERTIES OF MAGNETOPLASMONIC MICRODISCS

**© 2025 A. A. Anikin[a, *], A. Motorzhina[a], V. K. Belyaev[a], V. V. Rodionova[a], L. V. Panina[a,b]**

[a]*Immanuel Kant Baltic Federal University, Kaliningrad, Russia*

[b]*National University of Science and Technology "MISIS", Moscow, Russia*

**e-mail: anikinanton93@gmail.com*

Received November 15, 2024

Revised December 14, 2024

Accepted December 30, 2024

**Abstract.** We investigated the polarizability, optical density spectra, and photothermal properties of Au/Fe/Au and Fe/Au/Fe layered microdisks synthesized by lift-off optical lithography. An analytical method for determining the electric polarizability in the quasi-static approximation is proposed. Theoretical and experimental results are consistent in the visible and near-IR spectral ranges. The results obtained provide an assessment of the applicability of such microdisks for combined photothermal and magnetomechanical anticancer therapy.

**Keywords:** *layered microdisks, electrical polarizability, photothermia, hyperthermia, magnetomechanical stimulation*

**DOI:** 10.31857/S03676765250412e3

# INTRODUCTION

Magnetic particles (MPs) have a wide range of applications in the biomedical field, including cancer treatment using magnetic hyperthermia [1], or magnetically controlled delivery and release of antitumor drugs to the target area [2]. Recently, methods for cancer cell destruction based on the movement of magnetic particles in varying magnetic fields have been actively developed [3,4]. The most suitable materials should have high mechanical momentum under the influence of alternating magnetic fields. In particular, microdisks with a vortex magnetic structure in the ground state created by magnetron sputtering and subsequent optical lithography [5,6], nanowires and nanotubes obtained by electrochemical synthesis in porous membranes [7,8], ultrafine magnetic particles with perpendicular magnetization [9], and synthetic antiferromagnetic microdisks with zero residual magnetization are considered. The main difficulties in the preparation of such materials arise in obtaining stable colloidal solutions of nanoparticles with their optimal magnetomechanical and hysteresis properties, in reducing cytotoxicity, and in scaling up synthesis methods.

The use of only one method of action on cells may be insufficiently effective. It is of interest to study the joint action of mechanical forces and heating, both due to magnetic hyperthermia and photothermia [10-12]. However, magnetic materials are generally not well heated when interacting with light, especially in the near-infrared region, at wavelengths around 800 nm, which is the first window of transparency of biological tissues. On the other hand, in order to improve the biocompatibility and stability of PMs and to reduce their agglomeration, coatings of various biocompatible materials, including

gold, are used [13]. This leads to an increase in optical absorption and photothermal heating efficiency, which makes it possible to combine several anticancer therapies using the same type of particles. This is particularly relevant in the context of the emerging field of nanomedicine, where such particles can be used to generate local forces or moments on biological samples at different temperatures and study cellular response.

In this work, the optical properties of layered microdisks in two configurations Au/Fe/Au (AFA) and Fe/Au/Fe (FAF) fabricated by tear-off optical lithography were investigated. The first type of disks exhibits large optical absorption up to the IR region and photothermal efficiency. Whereas the second type has greater potential for use in magnetomechanical therapy.

## MATERIALS AND METHODS

### *Synthesis of AFA and FAF microdisks*

Microdiscs were synthesized at the FIC Krasnoyarsk Scientific Center of the Siberian Branch of the Russian Academy of Sciences. Layered metal disks were obtained by tear-off optical lithography combined with electron-beam deposition of metal layers. Before forming the polymer mask, Si(100) substrates were chemically cleaned and treated in $O_2$plasma to improve adhesion. A negative photoresist FN 16-4U (diluted with AZ EBR Solver to a thickness of 700-800 nm) was prepared to produce the mask. Application was performed at a centrifuge speed of 3000 rpm for 60 s. Drying steps were then performed for 60 s at 110° C (before and after the exposure procedure). The exposure time with radiation from a mercury lamp with an emission wavelength of 365 nm was 11 s. After

exposure for 20 s, a mask in the form of freestanding photopolymer columns was obtained. Before deposition of metal layers, a gentle 15 s treatment in $O_2$plasma at 150 W power and 20 $cm^3$/min gas flow was performed. The thickness of the metal layers was monitored using a quartz thickness meter.

To separate the disks from the substrate, the photoresist was dissolved using dimethyl sulfoxide (DMSO). Each wafer was treated individually in a beaker of appropriate diameter. For better efficiency and shorter processing time, the DMSO-coated wafers were placed on a heating plate (60-70 °C) for 15-20 min and then treated with ultrasound for 2-5 min. Microdiscs were collected using a permanent magnet and micropipette and placed in a glass vial. For further storage, the disks were washed and diluted with acetone. 2 types of disks with diameters of 1000±100 nm with different sequence of functional layers and their thicknesses (in nm) were synthesized by this method: Au(10)/Fe(70)/Au(10) and Fe(50)/Au(10)/Fe(50). Before the study, the disks were washed and diluted with distilled water.

The morphology of microdisks was studied on a Hitachi SU3500 scanning electron microscope by scanning electron microscopy (SEM) using a secondary electron detector (Everhart-Thornley detector). SEM images of a 20-30 μL drop of disk suspension in acetone dried on a Si(100) silicon substrate were obtained. Before drying, the microdisk suspension was placed in an Elmasonic S 15 H ultrasonic bath for 15 min at room temperature. The relative chemical content of elements was measured using a Bruker Quantax 75 energy dispersive spectrometer as part of a Hitachi TM4000 scanning electron microscope, the accelerating voltage was 15 kV.

*Optical polarizability of layered disks*

The problem of determining the polarizability of bodies of cylindrical shape, even in the electrostatic approximation, has no analytical solution. There are only a few geometrical figures that allow us to obtain analytical solution of the Laplace equation. Such figures include spheres, infinite cylinders with circular cross section (two-dimensional analog of a sphere), and ellipsoids. However, circular cylinders of finite length do not belong to them, although they are the basic shapes found in many canonical problems. In [14], numerical calculations of the dielectric polarizability of a circular cylinder were performed for different values of the length-to-diameter ratio ($l/d$ ). The numerical results were compared with the known results for the polarizability of a spheroid (ellipsoid of rotation) with the same ratio$l/d$ . The discrepancy did not exceed 1%.

Based on these results, layered disks are approximated by cofocus ellipsoids. Such a problem is solved within a single coordinate system$(\xi, \eta, \zeta)$ , based on the semi-axes of the inner ellipsoid$a_1 > b_1 > c_1$ , which are related to the Cartesian coordinates in the usual way [15]. The problem is easily generalized to an ellipsoid with *n* layers. The dielectric constant of the layers is$\varepsilon_i$ , and the dielectric constant of the external medium is$\varepsilon_{ex}$ . The semi-axes of the following ellipsoids are defined as

$$a_i^2 = a_1^2 + d_i, \quad b_i^2 = b_1^2 + d_i, \quad c_i^2 = c_1^2 + d_i \tag{1}$$

The condition$\xi = 0$ defines the surface of the inner ellipsoid. Next, consider the case when the external electric field$E_{in}$ is homogeneous and directed along the *z-axis*. The external field potential$\varphi_0 = -E_{in}z$ in ellipsoidal coordinates is defined as:

$$\varphi_0 = -E_{in}\left(\frac{c_1^2+\xi}{(a_1^2-c_1^2)(b_1^2-c_1^2)}\right)^{\frac{1}{2}} g(\eta,\zeta),\ g(\eta,\zeta) = \sqrt{(c_1^2+\eta)(c_1^2+\zeta)} \tag{2}$$

The potential$\varphi_i$ corresponds to the potential in the *i-th* layer, with$\varphi_1$ being the potential in the inner ellipsoid and$\varphi_{n+1}$ being the potential in the outer medium. The Laplace equation in ellipsoidal coordinates has the following form:

$$\Delta\varphi = (\eta - \zeta)f(\xi)\frac{\partial}{\partial\xi}\left(f(\xi)\frac{\partial\varphi}{\partial\xi}\right) + (\zeta - \xi)f(\eta)\frac{\partial}{\eta}\left(f(\eta)\frac{\partial\varphi}{\partial\eta}\right) +$$

$$+(\xi - \eta)f(\zeta)\frac{\partial}{\partial\zeta}\left(f(\zeta)\frac{\partial\varphi}{\partial\zeta}\right) = 0 \tag{3}$$

$$f(u) = ((a_1^2+u)(b_1^2+u)(c_1^2+u))^{1/2}, u = \xi,\eta,\zeta$$

The surfaces of the layers satisfy the equation$\xi = d_i$ , so the solution for the potential is in the form:

$$\varphi = F(\xi)g(\eta,\zeta) \tag{4}$$

The two linearly independent solutions for$F(\xi)$ are of the form:

$$F_1(\xi) = (c_1^2+\xi)^{1/2}, \qquad F_2(\xi) = F_1(\xi)\int_\xi^\infty \frac{du}{F_1(u)^2 f(u)} \tag{5}$$

Given the boundedness of the solution at the center and the zero reversal of the scattering potential$\varphi_s$ at infinity,$\varphi_1$ and$\varphi_{n+1}$ are written as:

$$\varphi_1 = A_1F_1(\xi), \quad -c_1^2 < \xi \le 0 \tag{6}$$

$$\varphi_{n+1} = \varphi_s + \varphi_0 = \left(B_sF_2(\xi) - E_{in}\frac{(c_1^2+\xi)^{\frac{1}{2}}}{((a_1^2-c_1^2)(b_1^2-c_1^2))^{\frac{1}{2}}}\right)g(\eta,\zeta),\ d_n < \xi < \infty \tag{7}$$

The parameter$B_s$ defines the polarizability of .$\chi$

The general solution for the potential in the *i-th* layer is as follows:

$$\varphi_i = \big(A_2F_1(\xi) + B_2F_2(\xi)\big)g(\eta,\zeta), \quad d_{i-1} < \xi \le d_i \tag{8}$$

The boundary conditions require continuity of the potentials and normal components of the electric induction vector *D.* These conditions are written as

$$\varphi_i = \varphi_{i+1}, \quad \frac{\varepsilon_i \partial\varphi_i}{\partial\xi} = \frac{\varepsilon_{i+1}\partial\varphi_{i+1}}{\partial\xi} \tag{9}$$

The system of equations (9) is divided into pairs, with the first and last pairs differing from the inner pairs, which have the standard form. This allows us to relate the parameters$A_1$ and$B_s$ by means of the product of characteristic matrices. For a two-layer ellipsoid with$a_1 = b_1, a_2 = b_2$ , the relation between the normalized parameter$\tilde{A}_1$ and the polarizability$\chi$ has the following form:

$$\tilde{A}_1\widehat{M}_2\widehat{M}_1{}^{-1}\begin{pmatrix}1\\ \varepsilon_1\end{pmatrix} = \begin{pmatrix} -1 + \frac{\chi}{\varepsilon_{ex}}N_{z,2} \\ -\varepsilon_{ex} + \frac{\chi}{\varepsilon_{ex}}\big(N_{z,2}-1\big)\big)\end{pmatrix}$$

$$\widehat{M}_1 = \begin{pmatrix}1 & 2N_{z,1}\\ \varepsilon_2 & 2\varepsilon_2\big(N_{z,1}-1\big)\end{pmatrix}, \widehat{M}_2 = \begin{pmatrix}1 & 2\delta N_{z,2}\\ \varepsilon_2 & 2\delta\varepsilon_2\big(N_{z,2}-1\big)\end{pmatrix}, \delta = \frac{b_1^2c_1}{b_2^2c_2} \tag{10}$$

$$N_{z,1,2} = \frac{1+\varepsilon_{1,2}^2}{\varepsilon_{1,2}^3}\big(\varepsilon_{1,2} - tan^{-1}\varepsilon_{1,2}\big), \varepsilon_{1,2} = \sqrt{\frac{b_{1,2}^2}{c_{1,2}^2} - 1}$$

For polarizability in the transverse direction (e.g., along the *x-axis*), the factors$N_{z,1,2}$ should be replaced by .$(1 - N_{z,1,2})/2$

The spectra of aqueous solutions of microdiscs were measured using a BWTek Exemplar fiber optic spectrometer. A ThorLabs SLS203F globar-based lamp was used as a light source.

The photothermal properties of aqueous microdisk suspensions were quantified by measuring the temperature during IR laser heating and subsequent cooling. A temperature-stabilized laser diode (L808P1000MM, ThorLabs) with a wavelength of 806 nm had an intensity of 2.4 W/cm$^2$with a total optical power output of 0.625 W. The diode power as well as the stability of the intensity stability of the light intensity passed through the solution during photothermal heating was analyzed using a photodiode in an integrating sphere (S142, ThorLabs). The volume of the cubic glass cuvette for nanoparticle suspensions was 1.9 mL. The cuvettes were hermetically sealed to prevent evaporation. The temperature of the suspensions was measured using an IR camera (CG640, COX). For better stability of nanoparticles, the surfactant sodium dodecyl sulfate (SDS) was added to the aqueous particle suspensions in an amount of 5% by weight.

## RESULTS AND DISCUSSION

### *Synthesis of AFA and FAF microdisks*

SEM images of the AFA and FAF microdisks are shown in Figure 1. The AFA samples were found to have an average linear size of 1000±100 nm, with surface roughness $R_q$= 3±1 nm and $R_a$= 2±1 nm (Figure 1a-1c). The number of gold atoms to the number of iron atoms relates approximately as 1:6. The samples prepared from aqueous suspension of FAF have a strong tendency to agglomerate when dried, making

quantitative analysis difficult, nevertheless, the samples were found to have an average linear size of 1000±100 nm and tend to form ~2-10 μm agglomerates, with surface roughness $R_q$= 31±10 nm and $R_a$= 24±10 nm (Fig. 1g-1e). The number of gold atoms to the number of iron atoms is approximately 1:17.

*Optical polarizability of layered disks*

Polarizability of microdisks will depend on the direction of light polarization relative to the disk plane. Figure 2 shows the spectral characteristics of the imaginary part of the electric polarizability for disks of both compositions. The optical constants for the dielectric constant of Au and Fe are taken from [16,17]. In aqueous suspensions, the microdiscs are oriented chaotically and both contributions will appear on the spectral characteristics simultaneously. When the electric field is directed perpendicular to the plane of the disks, peaks in the shorter wavelength region are observed for both compositions. The polarizability of the disks in the configuration when the electric field is directed along the surface (Fig. 2a) is much higher than the value for the perpendicular orientation (Fig. 2b). In the case of AFA, a well-defined peak at a wavelength of 765 nm is observed. For the FAF composition disks, there is a broad peak in the 650 nm region, which is due to the attenuation of the electromagnetic field in the upper Fe layers. Meanwhile, in both cases, the polarizability values in the infrared region remain high, i.e., a significant photothermal effect in the region of tissue transparency can be expected.

*Spectroscopy and photothermia*

Optical density spectra of microdisc suspensions at a concentration of 100 μg/mL are shown in Fig. 3a. Taking into account the absolute scale of optical density, the samples do not show a distinguished range of wavelengths at which a markedly increased absorption occurs. This is due to the random orientation of the particles in the suspension as well as their spontaneous agglomeration due to the presence of magnetization, which leads to broadening of the absorption and scattering peaks. The suspension of AFA microdiscs have about 1.5 times higher optical density over the whole investigated range than FAF, as expected from their polarizability modeling results. Broad peaks in the region around 600-700 nm for FAF and 700-900 nm for AFA are also seen, corresponding to the polarizability spectra presented above.

Aqueous suspensions of microdiscs demonstrate relatively good stability, not changing the optical density values during the spectroscopic measurement. However, they are not fully colloidally stable and on exposure times longer than 15 min they start to settle, changing the transmittance. This can be solved by coating with surfactants, leading to an increase in the Zeta potential and also preventing the interaction of the magnetic moments of the microdisks.

To determine the photothermal performance of microdiscs for photothermal therapy, it is not enough to study their spectroscopic characteristics alone. It is also necessary to obtain values of the fraction of light energy attenuated by microdisk suspensions, converted into thermal energy of the suspension, which is expressed by the photothermal conversion coefficient (η). This can be done by measuring the maximum heating temperatures and cooling rates of the suspension, when the laser is turned on and

off, respectively. In this case, it is possible to find the coefficient in the theormostatic equilibrium approximation [18]:

$$\eta = \frac{\sum_i m_i c_i \left(\frac{\Delta T_{max}}{\tau} - \frac{\Delta T^0_{max}}{\tau_0}\right)}{P_0(1-r)\left(1-\frac{I}{I_0}\right)}, \quad (11)$$

where $\sum_i m_i c_i$ is the total heat capacity of the cuvette with suspension, $\Delta T_{max}$ and $\Delta T^0_{max}$ are the maximum heating temperatures, and $\tau$ and $\tau_0$ are the characteristic cooling times of the microdisc suspension and the solvent without microdiscs, respectively. The characteristic time is found from the cooling curves as the exponent of the exponent. The reflection-corrected incident radiation power is $P_0(1-r)$ , and $\left(1-\frac{I}{I_0}\right)$ is the fraction of the attenuated incident radiation power by the suspension.

The time dependence of suspension temperature during laser heating is shown in Fig. 3b. AFA microdiscs coated with gold on the outside show higher heating temperatures at the same particle concentration of 100 μg/mL. The photothermal conversion coefficients calculated using expression (11) are 27±1 % and 30±1 % for AFA and FAF microdisks, respectively. The values of coefficients for layered microdiscs are slightly lower than those of plasmonic gold nanoparticles designed specifically for photothermia at the used wavelengths around 800 nm. However, they are higher than the usual values for magnetic nanoparticles. The presence of gold gives higher heating temperatures, while there is a possibility to influence the particles with a magnetic field. Also the presence of surfactant in the suspensions could affect the value of the coefficient, leading to greater turbidity of the solution, and consequently to greater scattering of

radiation. We also associate the lower value of the photothermal conversion coefficient of AFA microdisks with greater scattering of the gold layer compared to FAF.

## CONCLUSION

Thus, we studied layer microdisks obtained by tear-off optical lithography combined with electron-beam deposition of metal layers. By this method 2 types of disks with diameters of 1000±100 nm with different sequence of functional layers and their thickness (in nm) were synthesized: Au(10)/Fe(70)/Au(10) and Fe(50)/Au(10)/Fe(50). The optical absorption spectra were investigated. An analytical method was developed to calculate the dielectric polarizability of layer disks by approximating their shape with cofocus spheroids. The dielectric polarizability in an electric field along the surface of the disks is significantly larger than for perpendicular field direction for both types. For parallel polarization, the extinction remains high up to the IR region of the spectrum. When microdisk suspensions are exposed to near-IR laser radiation, they show relatively good heating degrees, exceeding those of magnetic particles without gold in their composition. The efficiency of IR radiation energy conversion into heat was 27±1 % and 30±1 % for AFA and FAF microdisks, respectively, which is quite good considering their significant optical absorption in this range. This study shows that layered microdiscs can be potential candidates for combined magnetomechanical and photothermal therapy.

## FUNDING

The research was financially supported by the Russian Science Foundation (project No. 21-72-20158). A. Motorzhina would like to thank the Strategic Academic Leadership

Program "Priority 2030" of I. Kant BFU (scientific project No. 123120500049-7) for the support of methodology development and microdisk photothermia research.

REFERENCES

1. *Kafrouni L., Savadogo O.* // Progr. Biomater. 2016. V. 5 P. 147.

2. *Oliveira H.*, *Pérez-Andrés E., Thevenot J. et al.* // J. Control. Release. 2013. V. 169. P. 165.

3. *Naud C., Thébault C., Carrière M. et al.* // Nanoscale Adv. 2020. V. 2. P. 3632.

4. *Golovin Y.I., Zhigachev A.O., Klyachko N.L. et al.* // Bull. Russ. Acad. Sci. Phys. 2018. V. 82. No. 9. P. 1073.

5. *Kim D. H., Rozhkova E.A., Ulasov I.V. et al.* // Nature Mater. 2009. V. 9. P. 165.

6. *Novosad V., Rozhkova E.A.* // In: Biomedical Engineering, Trends in Materials Science, 2011. P. 425.

7. *Contreras M., Sougrat R., Zaher A. et al.* // IJN. 2015. V. 10. P. 2141.

8. *Anikin A.A., Shumskaya E.E., Bedin S.A. et al.* // Bull. Russ. Acad. Sci. Phys. 2024. V. 88. No. 6. P. 1010.

9. *Mansell. R., Vemulkar T., Petit D.C.M.C. et al.* // Sci. Reports. 2017. V. 7. Art. No. 4257.

10. *Efremova M.V., Naumenko V.A., Spasova M. et al.* // Sci. Reports. 2018. V. 8. Art. No. 11295.

11. *Shi X., Tian Y., Liu Y. et al.* // Front. Oncol. 2022. V. 12. Art. No. 939365.

12. *Espinosa A., Kolosnjaj-Tabi J., Abou-Hassan A. et al.* // Adv. Funct. Mater. 2018. V. 28. Art. No. 1803660.

13. *Subekin A.Y., Pylaev T.E., Kukushkin V.I. et al.*// Bull. Russ. Acad. Sci. Phys. 2024. V. 88. P. 178.

14. *Venermo J., Sihvola A.* // J. Electrostat. 2005. V. 63. P. 101.

15. *Bohren C.F., Huffman D.R.* Absorption and Scattering of Light by Small Particles. N.Y.: Wiley, 1983. 533 p.

16. *Johnson P.B., Christy R.W.* // Phys. Rev. B. 1972. V. 6. P. 4370.

17. *Johnson P.B., Christy R.W.* // Phys. Rev. B. 1974. V. 9. P. 5056.

18. *Roper D.K., Ahn W., Hoepfner M.* // J. Phys. Chem. C. 2007. V. 111. P. 3636.

FIGURE CAPTIONS

Figure 1. SEM images obtained for samples with Au(10 nm)/Fe(70 nm)/Au(10 nm) (AFA) (a-c) and Fe(50 nm)/Au(10 nm)/Fe(50 nm) (FAF) (d-e) functional layer thicknesses.

Figure. 2. Polarizability spectra of AFA and FAF microdisks for the electric field directed along (a) and perpendicular (b) to the plane of the disks.

Figure 3. Experimental optical density spectrum of aqueous suspensions of AFA and FAF microdiscs taken at a concentration of 100 μg/mL (a); photothermal heating of aqueous suspensions of AFA and FAF microdiscs taken at a concentration of 100 μg/mL with the addition of SDS in an amount of 5% by weight (b).

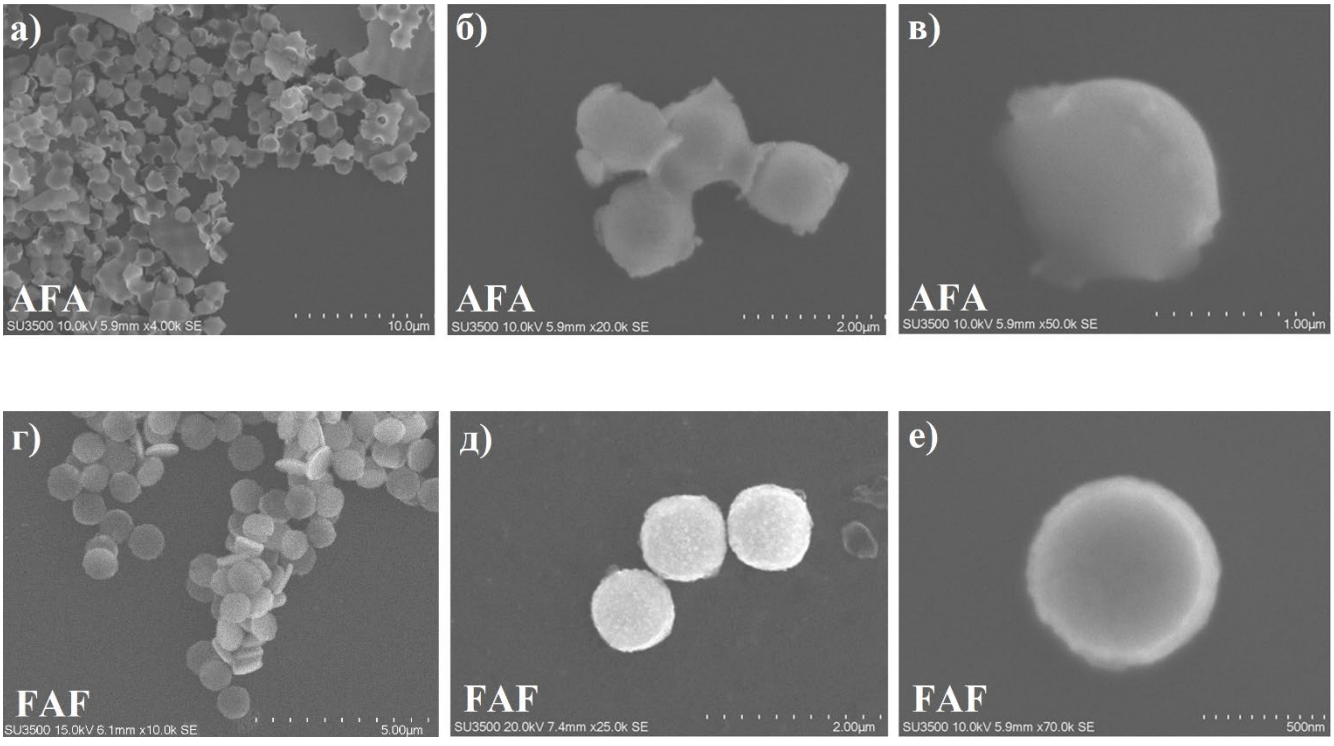


Fig. 1

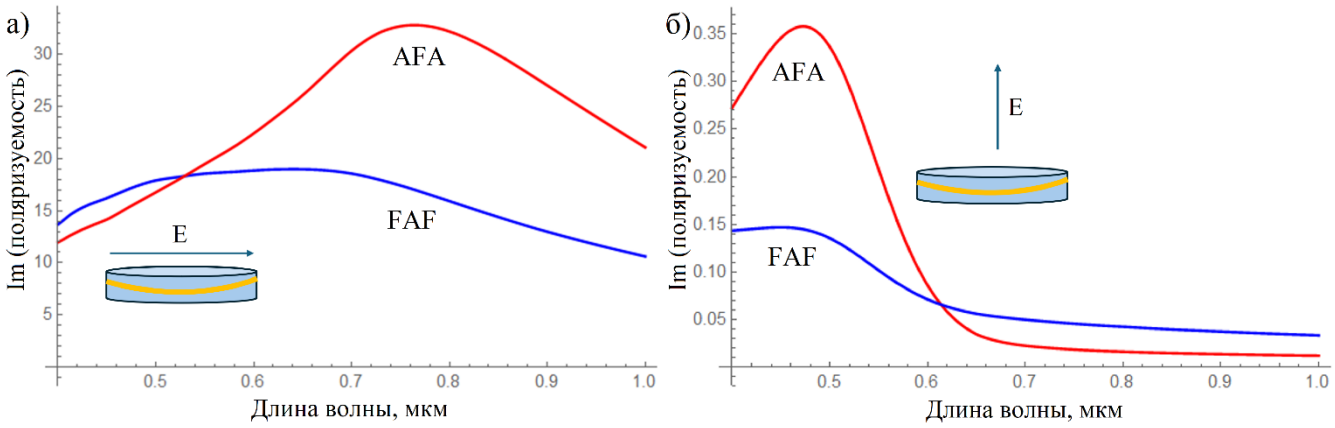
а)
б)
AFA
FAF
E
Im (поляризуемость)
Длина волны, мкм

Fig. 2

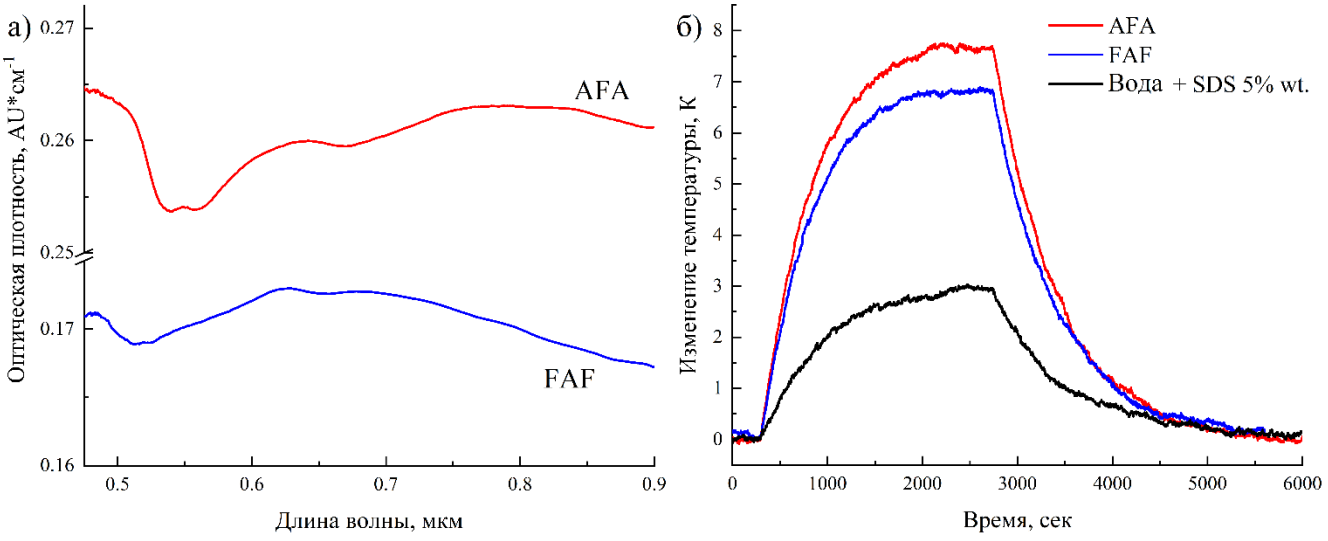
а)
б)
AFA
FAF
Вода + SDS 5% wt.
Оптическая плотность, AU*см-1
Изменение температуры, К
Длина волны, мкм
Время, сек

Fig. 3